COGEAR

MODULE 3:

Instrument evaluation, site selection, and installation of permanent instrumentation
Del. No.: 3b.1.3.2

Authors: Moore, J., Gischig V., Button, E., and Löw, S.

Engineering Geology, ETH Zürich

January 24, 2011

Task 3b.1.3

Instrument evaluation, site selection, and installation of permanent instrumentation

Deliverable: 3b.1.3.2

Jeffrey Moore, Valentin Gischig, Edward Button, and Simon Loew

Engineering Geology, ETH Zurich

Summary

This report summarizes instrument selection, installation, testing, and first results for new fiber optic strain sensors installed in COGEAR at the Randa test site. The described sensors have been chosen in order to meet special criteria for an earthquake monitoring system in Switzerland – i.e. earthquakes occurring during the study period are expected to be relatively small, and induced rock slope deformations may also be of small magnitude (scoping calculations placed expected displacements in the micrometer range). A system was therefore needed that could capture micrometer-scale movements at sampling rates appropriate for seismological investigations of ~100 Hz. The most suitable choice, within our budget, were fiber Bragg grating strain sensors.

With micro-strain resolution and the capability to sample at rates of 100 Hz and higher, fiber optic (FO) strain sensors offer exciting new possibilities for in-situ landslide monitoring. Here we describe a new FO monitoring system based on long-gauge fiber Bragg grating sensors installed at the Randa Rockslide Laboratory in southern Switzerland. The new FO monitoring system can detect sub-micrometer scale deformations in both triggered-dynamic and continuous measurements. Two types of sensors have been installed: (1) fully embedded borehole sensors and (2) surface extensometers. Dynamic measurements are triggered by sensor deformation and recorded at 100 Hz, while continuous data are logged every 5 minutes. Deformation time series for all sensors show displacements consistent with previous monitoring. Accelerated shortening following installation of the borehole sensors is likely related to long-term shrinkage of the grout. A number of transient signals have been observed, which in some cases were large enough to trigger rapid sampling. The combination of short- and long-term observation offers new insight into the deformation process. Accelerated surface crack opening in spring is shown to have a diurnal trend, which we attribute to the effect of snowmelt seeping into the crack void space and freezing at night to generate pressure on the crack walls. Controlled-source tests investigated the sensor response to dynamic inputs, which compared an independent measure of ground motion against the strain measured across a surface crack. Low frequency signals were comparable but the FO record suffered from aliasing, where undersampling of higher frequency signals generated spectral peaks not related to ground motion.

1. Introduction

In-situ monitoring of landslide displacements can be a critical means of evaluating the internal mechanisms and deformation characteristics of slope instabilities for hazard and risk assessment. Traditional in-situ sensors (e.g. mechanical or electrical extensometers) have long-established success for monitoring local movements, but are limited in the scope of their application by generally low resolution and sampling rates. Especially in the case of co-seismic slope deformations, traditional instruments are rarely capable of detecting small dynamic displacements, which are necessary data in conjunction with

local ground motion to better understand the seismic behavior of landslides (Harp and Jibson, 1995).

Fiber optic (FO) strain sensors are a promising new technology for advancing the state of the art in in-situ landslide monitoring. General performance advantages include high resolution, rapid sampling rate, multiplexing potential, and insensitivity to electrical disturbances (such as lightning). To date, however, there are only a few cases where FO strain sensors have been used for monitoring slope deformations in landslide investigations (notably Brunner et al., 2007; Woschitz and Brunner, 2008). Other applications of FO sensors in geoengineering include dynamic monitoring of tunnel displacements (Schmidt-Hattenberger et al., 1999; Nellen et al., 2000; Jobmann and Polster, 2007), rock deformation during laboratory testing (Schmidt-Hattenberger et al., 2003a; Wu et al., 2005), hydromechanical coupling during fluid injection (Cappa et al., 2006; Cappa et al., 2008), and geostructure performance (Inaudi and Casanova, 2000; Schmidt-Hattenberger et al., 2003b). Different types of FO sensors are available with varying resolution and cost. Fiber Bragg grating (FBG) sensors offer a good balance between performance and cost.

In this report, we describe a new FO monitoring system installed on the ground surface and in a deep borehole at the Randa rockslide. We describe the technical specifications, compare advantages and disadvantages of the system, highlight relevant first results and their implications, and compare FO time series data to that generated from traditional instruments already installed on site.

2. Randa Rockslide

In April and May of 1991, two consecutive rockslides occurred from a cliff high above the village of Randa in the Matter valley of Switzerland (Figure 1). These complex rockslides released a cumulative volume of approximately 30 million m^3 of crystalline rock, with each of the rockslide stages occurring over several hours (Schindler et al., 1993). Slide debris buried important transportation lines including the road and railway leading to Zermatt, and dammed the Mattervispa River which flooded a portion of the upstream town of Randa. No fatalities resulted from either rockslide event.

The Randa rockslide has been the subject of intensive research since its failure in 1991 (e.g. Schindler et al., 1993; Sartori et al., 2003; Eberhardt et al., 2004; Willenberg et al., 2008a,b). Around 5 million m^3 of rock above and behind the scarp of the 1991 rockslides remain unstable today, moving towards the valley at rates up to 20 mm/year (Gischig et al., 2009). Traditional in-situ and advanced remote sensing and geophysical techniques have been employed to investigate the mechanics and driving forces of the currently unstable rock mass and to construct a first kinematic model (Heincke et al., 2006; Spillmann et al., 2007; Willenberg et al., 2008a,b; Gischig et al., 2009). These investigations have yielded a great deal of information about the current rockslide deformation rates and patterns, but are limited by the resolution and low sampling rate of the traditional monitoring instruments. To extend and improve our monitoring strategy, with the added goal of understanding the rockslide's seismic response, we installed a fiber optic strain monitoring system based on long-gauge FBG sensors.

3. Monitoring System

3.1 Principle of Operation

Fiber Bragg gratings are short sections of optical fiber that contain a periodic variation in the index of refraction. When illuminated by broadband light, each FBG reflects a particular wavelength while transmitting all others undisturbed (Ferraro and de Natale, 2002). In this way, multiple sensors can be placed in series on the same optical fiber,

tuned at non-intersecting wavelength bands. The reflected wavelength is measured by an optical interrogator, and changes proportionally with the FBG strain within a linear regime.

3.2 System Components

Two types of FO strain sensors have been installed: (1) borehole sensors encased in grout at depths of 38, 40, and 68 m, and (2) crackmeters (crack extensometers) across tension cracks at the upper back surface of the rockslide (Figure 1). Borehole sensors were installed to span known active fractures showing normal mode offset previously identified with inclinometer, extensometer, and borehole video observations (Figure 2). Three borehole sensors in series make up one chain, and there are two identical chains (for redundancy) plus one unused chain for reserve. The borehole sensors are fully embedded in grout that extends up to 20 m depth in the borehole. An expanding grout was used to ensure good connection between the sensors and the pre-existing inclinometer casing into which they were installed. The two new fiber optic crackmeters at the top of the rockslide have been placed adjacent and parallel to existing vibrating wire crackmeters to allow for direct comparison. The FO crackmeters have both strain and temperature sensing FBG's, so the strain record can be compensated for changes in sensor temperature. They are anchored to the rock with aluminum L-brackets and inset steel masonry anchors, and shielded by an oversized aluminum cover. Each fiber optic sensor is encased in a flexible polyethylene tube that helps protect the sensor during transport and installation. The sensors may be submersed in up to 150 m of water.

The measurement system consists of the optical sensing interrogator (Micron Optics SM130) and the processing module (Micron Optics SP130). Our 4-channel model scans each of the active sensors at 100 Hz, and the data are placed into a circular buffer. The system is packaged with software from Smartec SA that allows for customizable data logging. One key feature of the data storage system is the capability to record both continuous (static) and triggered-dynamic measurements. Our system is configured to record one data point every 5 minutes (which is the average of all 100 Hz data during this time), while waiting for a set trigger threshold to be exceeded. In the event the trigger level is reached, the system records 5 seconds pre-trigger and 25 seconds post-trigger data at 100 Hz. The trigger is then rearmed while the continuous measurements proceed unaffected. The system can be remotely accessed via cellular modem in order to change acquisition parameters or download data.

The resolution capabilities of the FO system are defined by two parameters: repeatability and stability. Repeatability refers to the agreement between successive measurements under similar conditions over a short time period, while stability takes into account changes over the full operating temperature range of the device, as well as other long-term effects. The Micron Optics SM130 interrogator offers strain repeatability of better than 0.5 $\mu\varepsilon$ and stability of better than 2 $\mu\varepsilon$ (www.smartec.ch; www.micronoptics.com). Data averaging can greatly improve the measurement repeatability, if the noise is assumed to be random. For example, averaging N = 30,000 data points (100 Hz over 5 minutes) can improve the measurement repeatability by a factor of $N^{0.5}$ = 173 (Smith, 1997).

The sensor base length (or the distance between anchor points) controls both the absolute resolution and the measurement range over which the sensors behave linearly. Our *MuST* FBG sensors from Smartec SA have a measurement range of 0.75% of the base length in elongation and 0.5% of the base length in shortening. In general, we expect the borehole sensors to shorten and the surface crack sensors to elongate. Table 1 summarizes the sensor-specific resolution parameters based on the different sensor base lengths.

Each of the two active borehole sensor chains plus each of the two crackmeters has a dedicated cable running along the ground surface to the central measurement point

about 150 m distant. These armored cables consist of an optical fiber protected with stainless steel tubing, stainless steel reinforcing fibers, and a polyamide sheath. They have high mechanical and chemical resistance and are well suited for the harsh environment at the Randa rockslide.

The measurement system is contained within a small wooden hut built at 2410 m a.s.l. behind the crown of the rockslide (Figure 1). Since no grid power is available, all power is supplied by solar cells. Our solar system was designed to account for limited sunshine available during the winter months, combined with the likelihood of storms lasting several days. The combined continuous draw of the processing unit and interrogator was measured to be less than 50 W. Our power system has a total of 1160 W available from 12 photovoltaic panels, plus 1080 Ah of battery storage capacity.

3.3 Supporting Sensors

Other sensors installed at the Randa rockslide that support the FO strain measurements include traditional in-situ monitoring instruments such as in-place inclinometers (one unit at 12 m depth in the sb120 borehole), and vibrating wire (VW) crackmeters at coincident locations with the new FO instruments (cracks Z9 and Z10). Piezometers measure water pressure at the base of three boreholes, while a suite of meteorological sensors record air temperature, relative humidity, barometric pressure, total rainfall, and rock and soil temperature. Two broadband seismometers monitor local ground motion both within the unstable rockslide area and on adjacent stable ground (Figure 1), and a radio-synchronized clock ensures an accurate time reference for the FO system. Periodic geodetic surveys measure rockslide deformation using both regional and local base stations.

3.4 Integration of acquired data in the COGEAR and SwissEx IT platform

Data sharing within COGEAR is arranged through the COGEAR/SwissEx online GIS platform and GSN (http://sourceforge.net/apps/trac/gsn/). Sensor metadata – including sensor locations, types, resolution parameters, etc. – have already been implemented in the platform. The next step is to add up-to-date sensor data using GSN. A test installation with a server at EPFL was successful, and GSN access is prepared from a programming standpoint. What remains is to identify a permanent hardware and hosting solution. Sensor data to be shared include all strain measurements from the FO system, combined with all available meteorological data, updated at regular (weekly) intervals. Real-time data transfer and access is not yet possible.

Table 1: Resolution parameters for FO borehole and crack sensors. For measurement range "+" indicates elongation while "-" designates shortening.

Sensor	Base length	Repeatability	Stability	Measurement range
Borehole	1.5 m	0.7 μm	3 μm	+11 mm / -7.5 mm
Surface crack	0.8 m	0.4 μm	1.6 μm	+6 mm / -4 mm

4. Results

The FO monitoring system has been operational roughly 95% of the time since its installation at the end of August, 2008. Downtime over this period reflects a combination of software and internet connection problems combined with difficult winter site access.

4.1 Borehole Measurements

FO borehole sensors were emplaced to span known active fractures showing normal mode offset. The targeted fractures were previously characterized in borehole surveys, and slip rates determined from inclinometer and extensometer measurements (Willenberg et al., 2008b). The deepest fracture (68 m) dips approximately 50° and has a long-term shear rate of 2.8 mm/year, resulting in an axial shortening rate of 1.6 mm/year (Figure 2). The fracture at 40 m dips roughly 60° and shows an axial shortening rate of 0.3 mm/year, while the fracture at 38 m dips about 30° with an axial shortening rate of 0.5 mm/year. The upper two fractures may be part of a fault zone. The FO sensors measure only the component of deformation in the line of the sensor, or along the borehole axis. Therefore these sensors shorten (de-stress) over time.

From the displacement and velocity trends shown in Figures 3 and 4, we observe that all borehole sensors are shortening (negative extension values) as expected. Qualitatively, the rates of shortening match with previous INCREX extensometer surveys, wherein the deepest fracture at 68 m is found to deform the fastest, the fracture at 40 m has the slowest shortening rate, and the fracture at 38 m is intermediate between the other two (compare with Figure 2). Quantitatively, we find generally fair agreement between the current velocities and the previously measured long-term values (see inset table on Figure 4). Differences are likely due to the longer observation period for previous extensometer surveys (6 years) as compared to the reported ~1 year of FO monitoring, combined with temporary perturbation of the borehole area by the grouting and installation processes. Furthermore, the INCREX extensometer base length was 0.6 m, as compared to the 1.5 m base length FO sensor, so the FO sensors may intersect other nearby fractures with additional activity.

One distinct trend in the long-term displacement data is an accelerated phase of shortening immediately following sensor installation (Figures 3 and 4). These higher displacement rates likely result from curing and shrinkage of the grout. The sensors were fully embedded in an expanding grout with relatively rapid initial curing (i.e. a few hours). However, the curing process continues over the course of a few weeks or months as the concrete slowly looses water to the generally drier surroundings (Nawy, 2008). The result is long-term volumetric shrinkage termed drying shrinkage. From the displacement and velocity record, we estimate that our installation required between 2-3 months before this drying shrinkage ceased and the sensors attained equilibrium with the surrounding rock mass. This problem may be addressed in future installations by including an accelerating admixture in the grout design.

Notable in the displacement time series in Figure 3 are a number transient jumps or steps. Figure 5a shows an expanded view of one such event that occurred on April 28, 2009. The event was a rapid step in axial extension at the deepest sensor (68 m), contrasting to otherwise steady shortening. The step was large enough that it also triggered rapid sampling (Figure 5b). The combination of short and long-term observation offers relevant insight into the deformation process. Figure 5b reveals that the majority of deformation occurred through one rapid step lasting less than 1 s, but that deformation continued with a smaller, slower step then continuous extension over the remaining seconds of detailed observation. Returning to the long-term record (Figure 5a), we observe that slow residual extension persisted for several hours until normal shortening resumed. No regional seismicity was recorded at the time of this transient step, and no remarkable environmental conditions existed at the site. This step, and others like it, may result from the complex kinematic behavior of the various rockslide

blocks; i.e., the mode of displacement across the monitored fracture may change in response to intermittent mobilization of other nearby discontinuities (see Willenberg et al., 2008b). An alternative explanation, however, is that this transient simply resulted from fracturing of the intact grout surrounding the sensors and deformation resulting in local dilation. The origins of such transients should be resolvable with continued monitoring.

4.2 Crackmeter Data

The two new FO crackmeters were placed adjacent and parallel to existing vibrating wire crackmeters (Geokon model 4420; 0.7 m length) to allow for direct data comparison and validation. Data from crack Z9 are shown in Figure 6, where unfiltered FO data are compared to unfiltered data from the VW instrument. In general, we see an excellent match between the two sensor types, with very similar displacement trends shown. Some of the visible differences likely arise from each sensor's thermal response and the temperature corrections applied according to the manufacturer's recommendation.

With resolution two orders of magnitude better than the traditional VW instruments, the new FO crackmeters allow us to observe previously unidentified signals in the crack aperture data. In Figure 6, the long-term displacement trend shows an acceleration phase lasting from about April 1 to April 12, 2009, that is unique to crack Z9. Previous VW crack monitoring revealed similar brief periods of acceleration repeated annually around the time of local snowmelt. Analyzing this section of the FO crack data in detail (Figure 7), we find a unique step-like pattern with a daily period, marked by accelerated opening at night and a slower rate of opening (sometimes nearly zero) during the day. This unique displacement trend is not seen elsewhere in the crack time history. At this particular time of year, the crack is covered by about 2 m of snow, so no daily temperature changes reach the sensors, and sensor thermal effects may be disregarded. The temperature at the base of the snow pack was observed to be nearly constant at -0.2 °C throughout the acceleration phase. This time of year is, however, coincident with the onset of above zero average air temperatures, sunny days, and intense snowmelt. We hypothesize that meltwater generated during the day seeps through the snow pack and into the soil that fills the space between the crack walls. This soil material has collapsed into the crack from the adjacent hillslope, and is a wedge-shaped body approximately 0.5 m wide and a few meters deep. At night, the supply of meltwater is cut off and water in the soil pore space may freeze, resulting in an expansive pressure against the crack walls and accelerated crack opening. The next day, new meltwater seeps down into the soil and begins to melt interstitial ice, relieving the wall pressure and slowing the rate of crack opening. This diurnal displacement pattern persists for nearly two weeks and returns briefly later in the month during another period of intense snowmelt. The pattern is not seen at crack Z10, which has a different geometry and rock blocks, rather than soil, filling the crack space.

The long-term trend of tension crack aperture is a function of both large-scale rockslide deformation and near-surface seasonal thermoelastic effects. On the diurnal time scale, thermoelastic expansion and contraction of the crack walls creates an additional aperture response. When the sensors are covered by 1 m or more of snow, such diurnal thermally-induced displacements vanish (compare winter and summer months, Figure 6). The full effect of near-surface thermoelastic strains will be explored in detail in an upcoming publication.

4.3 Dynamic Tests and Sensor Response

The suitability of FBG sensors for measuring dynamic displacements associated with passing seismic waves has been validated in both the laboratory and field (Schmidt-Hattenberger et al., 1999; Barrera, 2001; Schmidt-Hattenberger et al., 2003c; Wu et al., 2005). Here we present results of a controlled-source experiment designed to investigate the response of one FO crackmeter to local ground motion. We compare an independent

measure of ground motion with the dynamic strain measured across the crack by the FO sensor.

Two 3-component geophones were placed directly adjacent to each of the crackmeter anchor points (0.8 m apart), securely attached to the exposed bedrock on each side of the crack. These 4.5 Hz geophones were read at 16 kHz by a Geometrics Geode datalogger independent from the FO system. All geophones were leveled and aligned so that one horizontal component was parallel to the crackmeter. Ground vibration was stimulated by a shotgun source, which used 10-gauge blank shells set in nearby shallow holes. The distance between the shot points and the crack was varied between 1 and 3 m. Shots at 1 m generated the clearest FO signals but the seismic records were badly clipped. Shots at 2 m were a good balance between the FO and seismic system capabilities, with minimal clipping and generally good FO signal quality. Shots at 3 m generated only small changes in crack aperture with poor FO signal waveforms. Geophones measure ground velocity, so the records were integrated with respect to time to obtain ground displacement.

Seismic measurements showed that ground motion on the crack wall opposite from the shot was insignificant, so we consider this area stable. Therefore, we compare the horizontal, inline ground motion from the geophone on the crack wall adjacent to the shot with the measured FO displacement. Figure 8a shows both the dynamic ground displacement and crack aperture change for a shot at 2 m distance. Generally good agreement can be observed between the time series response of the independent sensors, especially in the low frequency response. The maximum change in crack aperture is 11 μm, while the peak ground displacement is around 4 μm. This discrepancy likely arises from the few clipped velocity peaks in the beginning of the geophone time history that result in underestimation of the displacement magnitude at early times. High frequency energy generated from the shot can be observed within the first 0.1 s, which is undersampled and poorly represented by the FO displacement record. Following this initial phase, the FO sensor appears to ring for the next ~0.4 s until the signal falls below the measureable level. The low frequency ground motion is represented well by the FO strain measurements, while the higher frequency components cannot be measured accurately (as expected for 100 Hz sampling).

Figure 8b compares the spectra of the fiber optic strain signal to that of the recorded ground motion. The data shown are the stacked average values of five total shots at 2 m, which were found to have a consistent frequency response. Peaks in the fiber optic strain record are seen at 3.5, 8, 16, and 38 Hz, while the ground motion shows primarily a broad peak centered at 4 Hz. The low-frequency components of both the FO and seismic measurements are in reasonably good agreement. However, significant peaks in the FO response appear at 8, 16, and 38 Hz, which are not found in the ground motion spectrum. These are assumed to be instrument response, and we next examine possible sources of these peaks.

The fundamental resonant frequency (f_1) of the tightened optical fiber can be estimated by conceptualizing it as a stretched string and computing the transverse wave velocity:

$$f_1 = \frac{v}{2L} \tag{1}$$

where L is the sensor base length (0.8 m) and v is the wave velocity:

$$v = \sqrt{\frac{F}{\rho A}} \tag{2}$$

Here, A is the cross-sectional area of the optical fiber (0.0165 mm^2), ρ is its density (2200 kg/m^3), and F is the tensional force applied to the fiber (Barrera, 2001). F can be determined as:

$$F = EA\varepsilon \qquad\qquad\qquad\qquad\qquad\qquad (3)$$

where ε is the applied strain (~0.006 for the tightened crack sensor) and E is the Young's modulus of the optical fiber (~60 GPa; personal communication Luca Manetti). With these values, we calculate the fundamental frequency of the tightened fiber to be about 250 Hz, which is much larger than our measured response.

The fundamental frequency of the polyethylene (PE) tube that surrounds and protects the optical fiber can be estimated in the same manner as above (Eq. 1-3). Using a Young's modulus of 0.91 GPa, strain of 0.006, and a density of 940 kg/m^3 (personal communication Luca Manetti), we find that the fundamental frequency of the tightened PE tube is around 50 Hz. This value is again larger than our observed spectral peaks.

Vibration of the crackmeter anchor may explain some of the resonance observed, since the particular anchor sits about 30 mm above the rock surface on top of a 10 mm diameter steel rod. This configuration was chosen to keep the optical fiber level between the two anchors and perpendicular to the direction of crack opening. Analyzing the anchor as a single-degree-of-freedom system suggests, however, that its fundamental frequency should be in the range of a few kHz, which is again much larger than our measured response.

The above-mentioned three sources of potential sensor vibration all showed resonant frequencies larger than the observed peaks in the FO spectrum (Figure 8b), meaning that no single source can be directly linked to these peaks. However, low-frequency aliases of higher-frequency signals can generate false peaks in the spectrum (Smith, 1997). Aliasing results from undersampling of waves with frequencies greater than the Nyquist frequency (50 Hz in our case). Often anti-aliasing filters can be applied at analog-to-digital conversion, but this is not possible in our fiber optic system. The energy produced by the shotgun source is rich in high-frequency energy, especially at these close distances, and many combinations of higher frequency waves can result in 8, 16, and 38 Hz signals when sampled at 100 Hz. Therefore, we conclude that during these controlled tests using a shotgun source, our dynamic FO signals are adversely affected by aliasing. Typically however, earthquakes are not rich in high-frequency energy, especially at the Randa rockslide where large attenuation is expected (Spillmann et al., 2007). Therefore, we expect that the FO sensors will provide accurate measurement of dynamic strain accompanying an earthquake.

5. Discussion and Conclusions

In this work we document the capabilities of fiber optic strain measurement in landslide monitoring applications, with special emphasis on dynamic deformation signals. After more than one year of operation at the Randa rockslide in southern Switzerland, our FO system had recorded a number of interesting short- and long-term signals that revealed partial details of the deformation mechanisms. Resolving displacements of less than 1 μm is now possible, allowing us to detect rockslide movements over the course of a few seconds to a few hours.

After installation, our borehole sensors experienced an extended (2-3 month) phase of accelerated shortening that we attribute to long-term drying shrinkage of the grout (Figures 3 and 4). To resolve this problem in the future, an accelerating agent could be added to the grout mixture, though high temperatures generated during curing should be avoided. Following the curing phase, the borehole sensors experienced axial shortening accompanying normal mode offset along steeply-dipping active fractures.

Measured rates of shortening are consistent with previous extensometer survey data (Figure 4). An annual trend is loosely apparent in the borehole data (see especially the sensor at 40 m), showing greater rates of shortening in the winter and slower rates during the summer months. This trend is confirmed by previous data from vibrating wire in-place inclinometers (Willenberg et al., 2008b) and will be investigated further in an upcoming publication. A number of transient signals indicate periods of rapid extension that contrast against the otherwise steady shortening (Figures 3 and 5). We have proposed a kinematic mechanism where the normal block toppling observed is interrupted, and the fracture displacement vectors altered, by intermittent mobilization of other nearby discontinuities; consistent with the geological model of Willenberg et al., 2008b. Until now, it has not been possible to resolve such small displacements in order to identify this local intermittent motion. We acknowledge, however, that these transient signals may also reflect break up of the grout within the borehole, and thus represent only local perturbations rather than large-scale rockslide deformation mechanisms. Since installation there have only been a few triggered events and no false triggers related to noise, confirming that the triggers are operating effectively and the levels are set appropriately.

New FO crackmeters on the surface of the rockslide show a complex long-term trend that is the combination of both near-surface thermal effects and rockslide deformation (Figure 6). A brief period of accelerated crack opening in the spring was investigated in detail and found to consist of a daily pattern where movements are greatest at night and slower during the day (Figure 7). We explain this displacement pattern through the effect of snowmelt seeping into the soil that fills the crack space, which then freezes during the night and generates localized expansive pressure on the crack walls. The trend only occurs during times of rapid snowmelt, which is confirmed by borehole piezometer data. The observed crack displacements are irreversible, in that the ice-induced opening is not recovered during successive melting periods.

Dynamic tests designed to explore the sensor response were performed for one of the FO crackmeters. These tests compared the dynamic crack aperture response to an independent measured of ground motion generated from a shotgun blast (Figure 8). Results revealed that low-frequency signals are represented well by the FO sensor, but that the fiber optic record suffers from aliasing of higher frequency energy (greater than 50 Hz) which generates apparent signals and false spectral peaks not related to ground motion. In the event of an earthquake, however, such high-frequency energy will not be present and the FO sensors are expected to provide accurate measures of dynamic strain. For monitoring higher frequency vibrations, FO interrogators with faster sampling rates are available.

The primary performance advantage of FO strain monitoring systems is the improvement in resolution and accuracy. Our system resolution is about two orders of magnitude better than that of the high-quality traditional sensors installed at the site (Table 1), and rapidly improves with data averaging. We can easily detect sub-micrometer deformations in the long-term record, which allows us, for example, to resolve daily strain patterns or small transients associated with different deformation processes. The possibility of triggered 100 Hz sampling offers the advantage of being able to capture dynamic deformations associated with passing seismic waves, and will enable us to investigate the seismic performance of the unstable rock mass. Higher sampling rates up to 1 kHz are also now available. Fiber optic systems have the general advantage of being insensitive to electrical disturbances such as lightning, which can be a significant source of difficulties for field applications. Furthermore, the optical cabling is robust and suitable for use in harsh landslide environments. Finally, the FBG system offers the possibility to place many sensors on only a few cables, which makes for easier and more secure installations.

The primary disadvantage of FO strain systems is cost. These systems are several times more expensive than their traditional in-situ monitoring counterparts. Another drawback is the relatively large power consumption, which in our case is roughly 50 W and required construction of a large solar array. Installation of the FO sensors proved to be relatively easy, but as with any new application certain challenges arose. At Randa, because we installed the borehole sensors into an existing inclinometer casing we wanted to use an expanding grout to ensure secure contact at this interface. However, this prompted concerns that high swelling pressures could damage the sensors, and led us to carefully consider the choice and quantity of expanding agent. Ultimately, the sensors were undamaged. Finally, it is important to note that the FO sensors have a limited range (Table 1), and after straining beyond this point they become inaccurate, inoperable, and can even break. This is a problem primarily for long-term monitoring applications, and can be alleviated by installing the sensors so that the base length can be readjusted, or by choosing a longer sensor base length.

References

Barrera, S.L. (2001). A deformation measurement system for dynamic structural monitoring, Ph.D. Thesis No. 2441, EPFL, Lausanne, Switzerland.

Brunner, F.K., Woschitz, H., and Macheiner, K. (2007). Monitoring of deap-seated mass movements, Proceedings 3rd International Conference on Structural Health Monitoring of Intelligent Infrastructure.

Cappa, F., Guglielmi, Y., Gaffet, S., Lançon, H., and Lamarque, I. (2006). Use of in situ fiber optic sensors to characterize highly heterogeneous elastic displacement fields in fractured rocks, International Journal of Rock Mechanics & Mining Sciences, 43(4) 647–654.

Cappa, F., Guglielmi, Y., Rutqvist, J., Tsang, C.-F., and Thoraval, A. (2008). Estimation of fracture flow parameters through numerical analysis of hydromechanical pressure pulses, Water Resources Research, 44, W11408, doi:10.1029/2008WR007015.

Eberhardt, E., Stead, D., and Coggan, J.S. (2004). Numerical analysis of initiation and progressive failure in natural rock slopes - the 1991 Randa Rockslide, International Journal of Rock Mechanics and Mining Sciences, 41, 69–87.

Ferraro, P. and de Natale, G. (2002). On the possible use of optical fiber Bragg gratings as strain sensors for geodynamical monitoring, Optics and Lasers in Engineering, 37, 115-130.

Gischig, V., Loew, S., Kos, A., Moore, J.R., Raetzo, H., Lemy, F., and Rivolta, C. (2009). Identification of active release planes using ground-based differential InSAR at the Randa rock slope instability, Switzerland, Natural Hazards and Earth Systems Sciences, 9(6), 2027-2038.

Harp, E.L. and Jibson, R.W. (1995). Seismic instrumentation of landslides: Building a better model of dynamic landslide behavior, Bulletin of the Seismological Society of America, 85(1), 93-99.

Heincke, B., Maurer, H., Green, A.G., Willenberg, H., Spillmann, T., and Burlini, L. (2006). Characterizing an unstable mountain slope using shallow 2- and 3-D seismic tomography. Geophysics, 71(6), B241-B256.

Inaudi, D. and Casanova, N. (2000). Geo-structural monitoring with long-gage interferometric sensors, Proceedings SPIE Conference on Nondestructive Evaluation and Health Monitoring of Aging Infrastructure.

Jobmann, M. and Polster, M. (2007). The response of Opalinus clay due to heating: A combined analysis of in situ measurements, laboratory investigations and numerical calculations, Physics and Chemistry of the Earth, 32, 929-936.

Nawy, E.G. (2008). Concrete construction engineering handbook. CRC Press, Boca Raton, FL.

Nellen, P.M., Frank, A., Brönnimann, R., and Sennhauser, U. (2000). Optical fiber Bragg gratings for tunnel surveillance, Proceedings Smart Structures and Materials 2000: Sensory Phenomena and Measurement Instrumentation for Smart Structures and Materials, 263-270.

Sartori, M., Baillifard, F., Jaboyedoff, M., and Rouiller, J.-D. (2003). Kinematics of the 1991 Randa rockslides (Valais, Switzerland), Natural Hazards and Earth System Sciences, 3, 423–433.

Schindler, C., Cuenod, Y., Eisenlohr, T., and Joris, C.-L. (1993). Die Ereignisse vom 18 April und 9 Mai 1991 bei Randa (VS) – ein atypischer Bergsturz in Raten, Eclogae Geologicae Helvetiae, 86(3), 643-665.

Schmidt-Hattenberger, C., Borm, G., and Amberg, F. (1999). Bragg grating seismic monitoring system, Proceedings SPIE Conference on Fiber Optic Sensor Technology and Applications, 417-424.

Schmidt-Hattenberger, C., Naumann, M., and Borm, G. (2003a). Fiber Bragg grating strain measurements in comparison with additional techniques for rock mechanical testing, IEEE Sensors Journal, 3(1), 50-55.

Schmidt-Hattenberger, C., Straub, T., Naumann, M., Borm, G., Lauerer, R., Beck, C., and Schwarz, W. (2003b). Strain measurements by fiber Bragg grating sensors for in-situ pile loading tests, Proceedings Smart Structures and Materials 2003: Smart Sensor Technology and Measurement Systems, 289-294.

Schmidt-Hattenberger, C., Naumann, M., and Borm, G. (2003c). Dynamic strain detection using a fiber Bragg grating sensor array for geotechnical applications, Proceedings European Workshop on Smart Structures in Engineering and Technology, 227-232.

Smith, S.W. (1997). The scientist and engineer's guide to digital signal processing. California Technical Publishing, San Diego.

Spillmann, T., Maurer, H.R., Heincke, B., Willenberg, H., and Green, A.G. (2007). Microseismic monitoring of an unstable rock mass. Journal of Geophysical Research, 112, B07301.

Willenberg, H., Loew, S., Eberhardt, E., Evans, K., Spillmann, T., Heincke, B., Maurer, H-R., and Green, A. (2008a). Internal structure and deformation of an unstable crystalline rock mass above Randa (Switzerland): Part I – Internal structure from integrated geological and geophysical investigations, Engineering Geology, 101, 1-14.

Willenberg, H., Evans, K.F., Eberhardt, E., Spillmann, T., and Loew, S. (2008b). Internal structure and deformation of an unstable crystalline rock mass above Randa (Switzerland): Part II – Three-dimensional deformation patterns, Engineering Geology, 101, 15-32.

Woschitz, H. and Brunner, F.K. (2008). Monitoring a deep-seated mass movement using a large strain rosette, Proceedings 13th FIG Symposium on Deformation Measurements and Analysis.

Wu, X.-D., Schmidt-Hattenberger, C., Krüger, K., and Chen, J. (2005). Temperature-controlled fiber Bragg grating dynamic strain detection system, Sensors and Actuators, A119, 68-74.
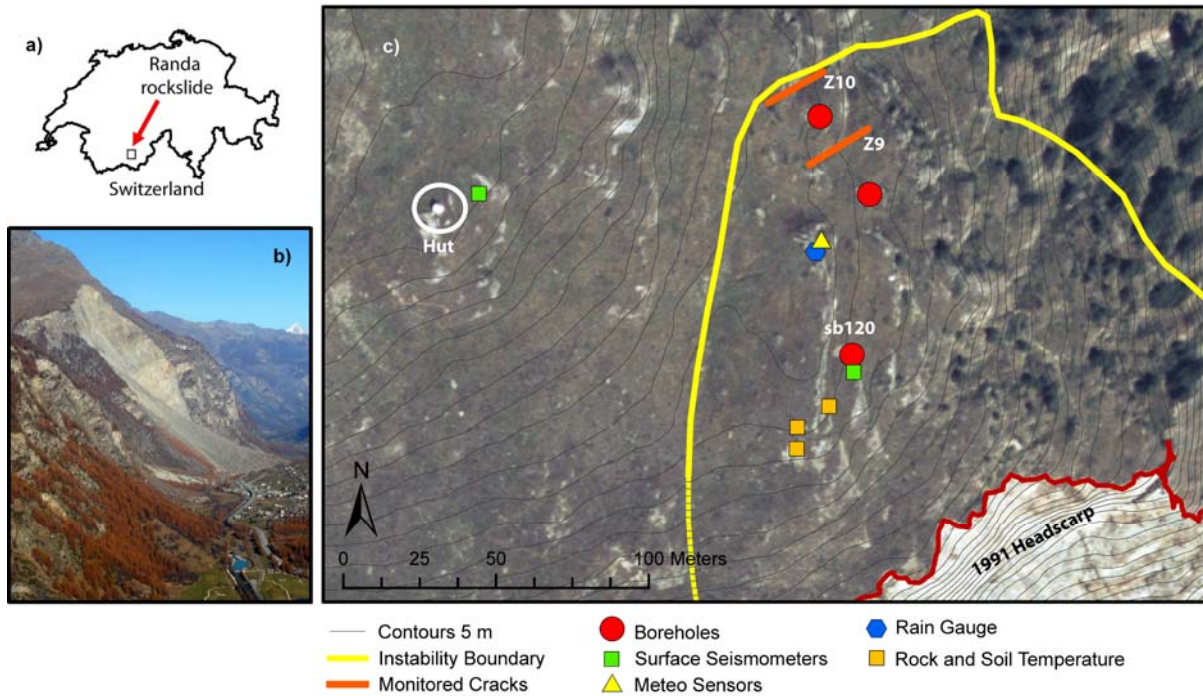
Figure 1: a) Location of the Randa rockslide, b) Overview of the rockslide and deposit in the Matter valley, c) Layout of the fiber optic strain sensors (borehole sb120, and cracks Z9 and Z10) and supporting sensors at the top of the currently unstable rock mass. For more details on the structure and kinematics of the unstable rock mass, see Willenberg et al., 2008a,b and Gischig et al., 2009.
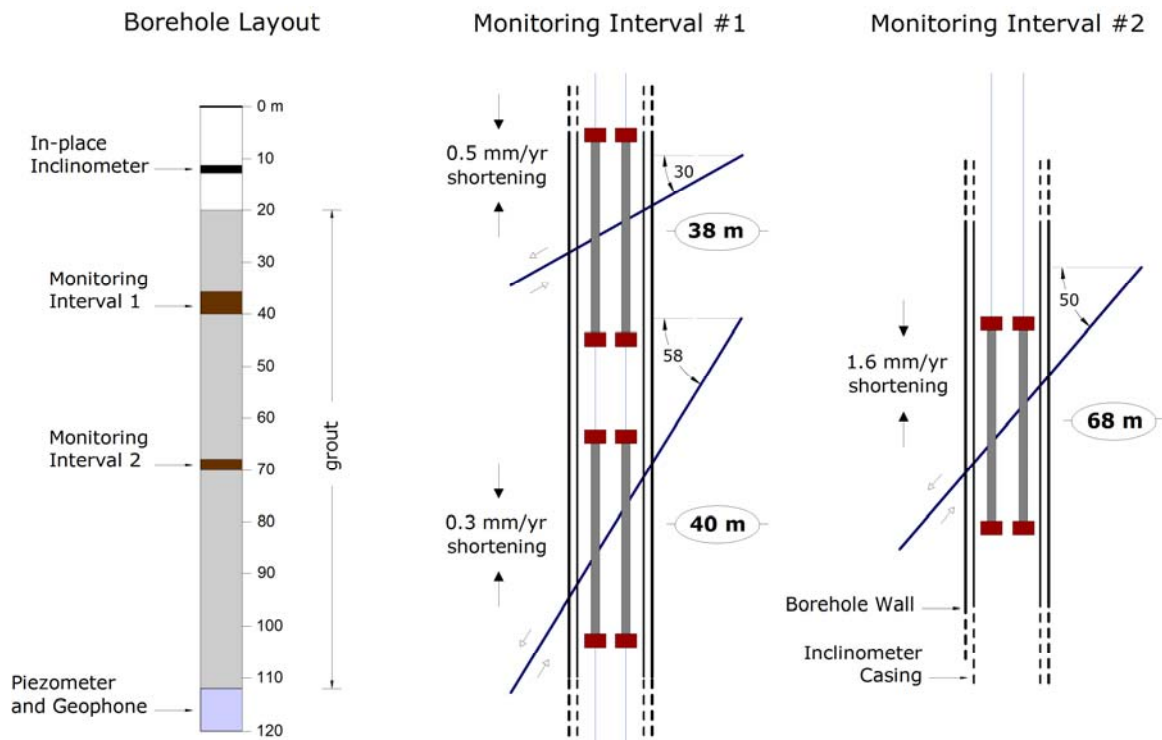
Figure 2: Detail of fiber optic sensor installation in borehole *sb120*. Two monitoring intervals were selected to span three active fractures showing normal mode offset (see slip arrows). The expected rates of shortening, calculated from previous extensometer surveys, are shown. Two active parallel sensor chains were installed for redundancy and security, and a third inactive chain (not shown) acts as reserve.

Figure 3: Deformation time series measurements from the three sensors at different monitoring intervals in borehole sb120 (data from just one sensor chain are shown). All sensors are shortening as expected. Accelerated shortening is seen immediately following sensor installation, which likely results from shrinkage of the grout. A number of transient steps and drops occur throughout the time history; one event from April 28, 2009 is highlighted in Figure 5. Dates are m/d/y.
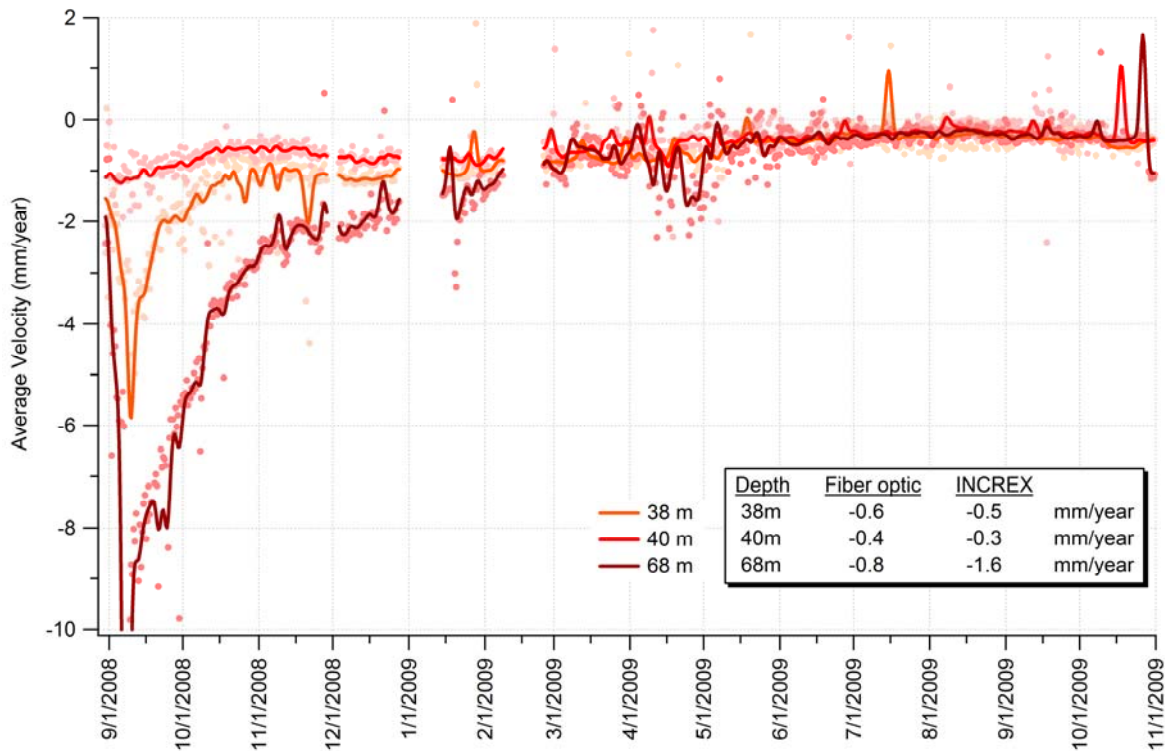
Figure 4: Velocity time series for the different sensors in borehole sb120. Dots indicate calculated half-day average velocities, while the solid lines are the data filtered with a binomial smoothing algorithm. The inset table shows comparison of the long-term average velocities with those determined from previous INCREX extensometer surveys. Accelerated shortening is clearly visible in the first 2-3 months of operation. Dates are m/d/y.
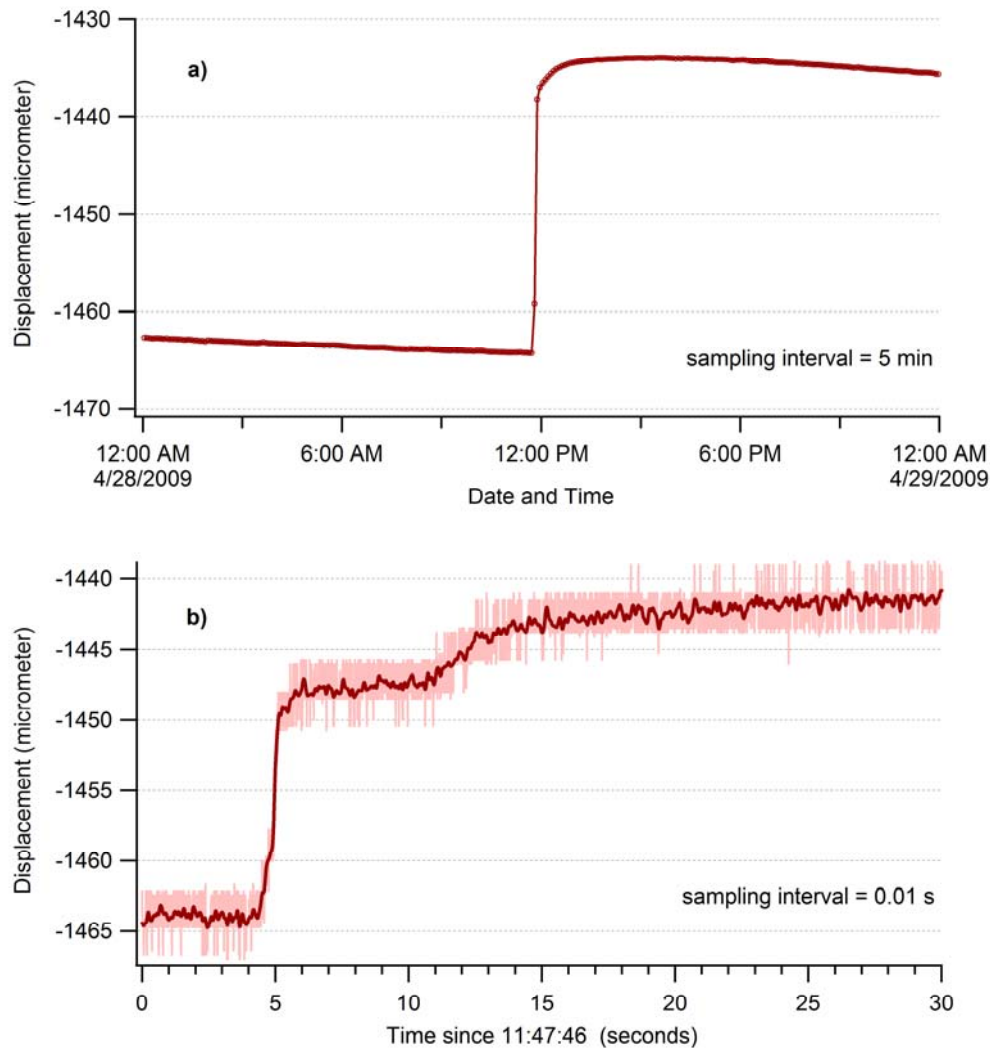
Figure 5: a) Expanded view of the transient step occurring on April 28, 2009. The event was a rapid period of axial extension amounting to about 30 μm at the deepest sensor (68 m), contrasting to otherwise steady shortening (see Figure 3). b) The step was large enough to also trigger rapid 100 Hz sampling. Observed details indicate that the majority of deformation occurred through one large step lasting roughly 1 s, and that deformation continued with a smaller, slower step followed by slow continuous extension.
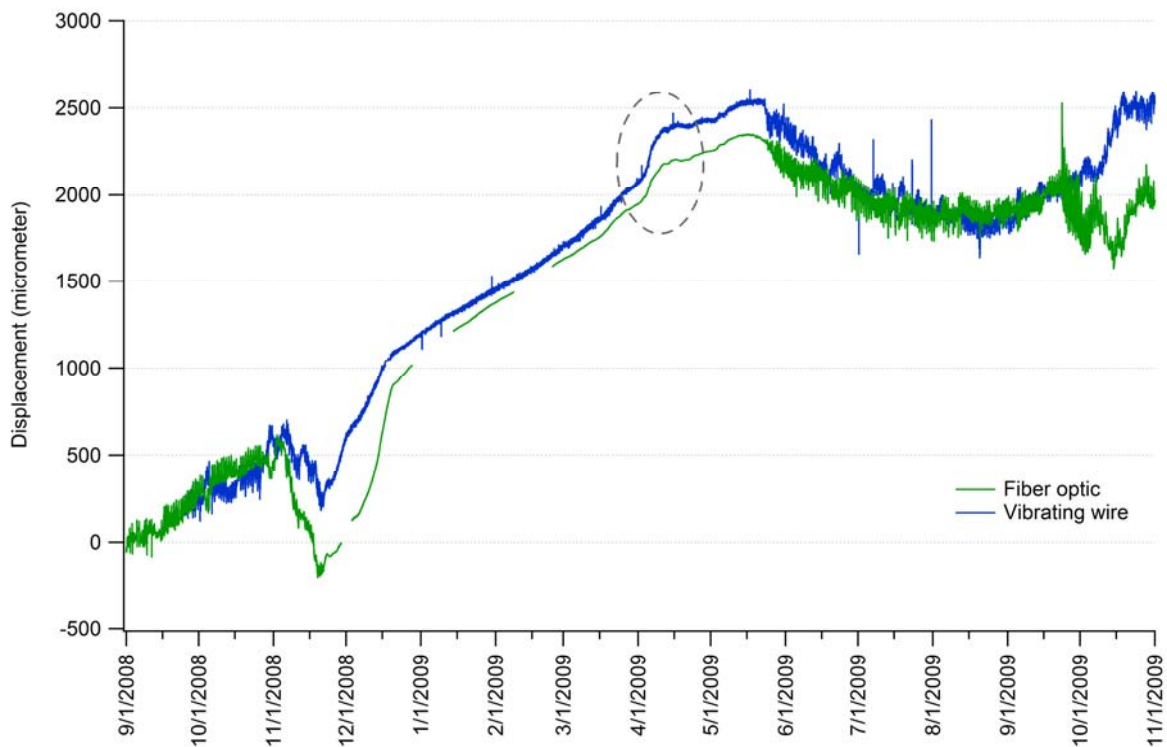
Figure 6: Unfiltered fiber optic crackmeter data compared with the time series from the traditional vibrating wire instrument. There is generally good match between the two sensor types, with very similar long-term displacement trends. Some differences likely arise from each sensor's thermal response and the applied temperature correction. The brief acceleration in April is circled and a select portion shown in detail in Figure 7. Dates are m/d/y.
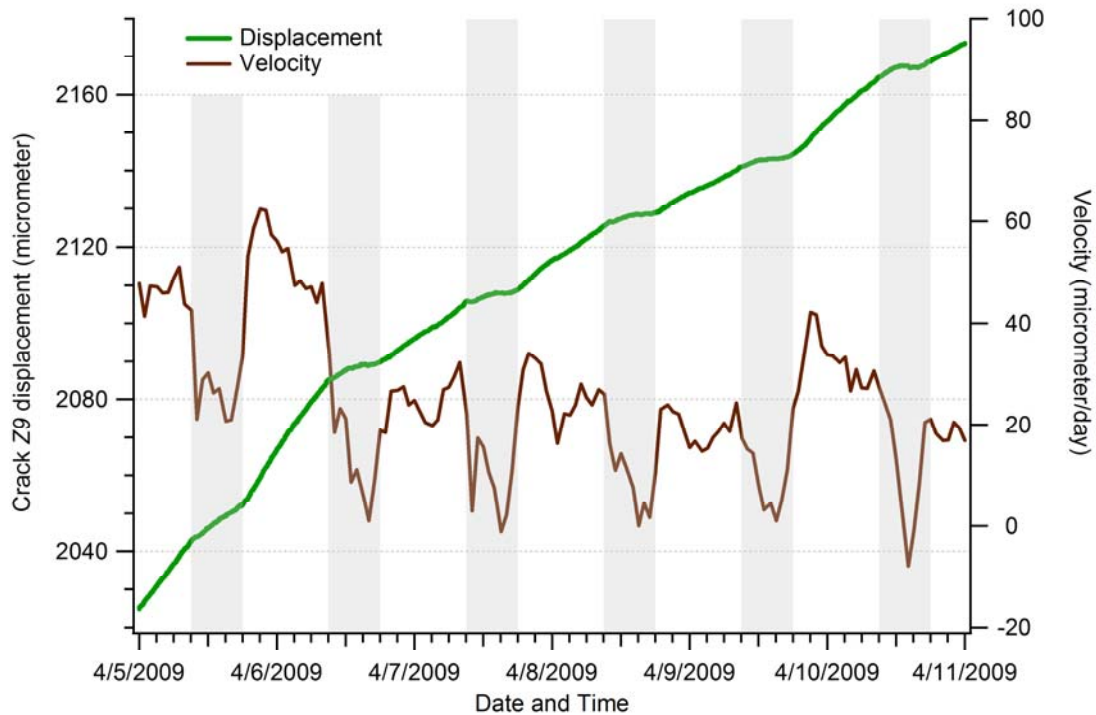
Figure 7: Detail of the brief period of accelerated opening at crack Z9 during April, 2009. Daytime hours from 9am to 6pm are shaded. Deformation data show a step-like pattern with a daily period, marked by accelerated opening at night and a slower rate of opening during the day. The occurrence is coincident with the onset of intense snowmelt, and the deformation response may reflect freezing of soil pore water during the night with accompanying increased wall pressure, followed by daily infiltration-induced melting and relief of wall pressure. Dates are m/d/y.
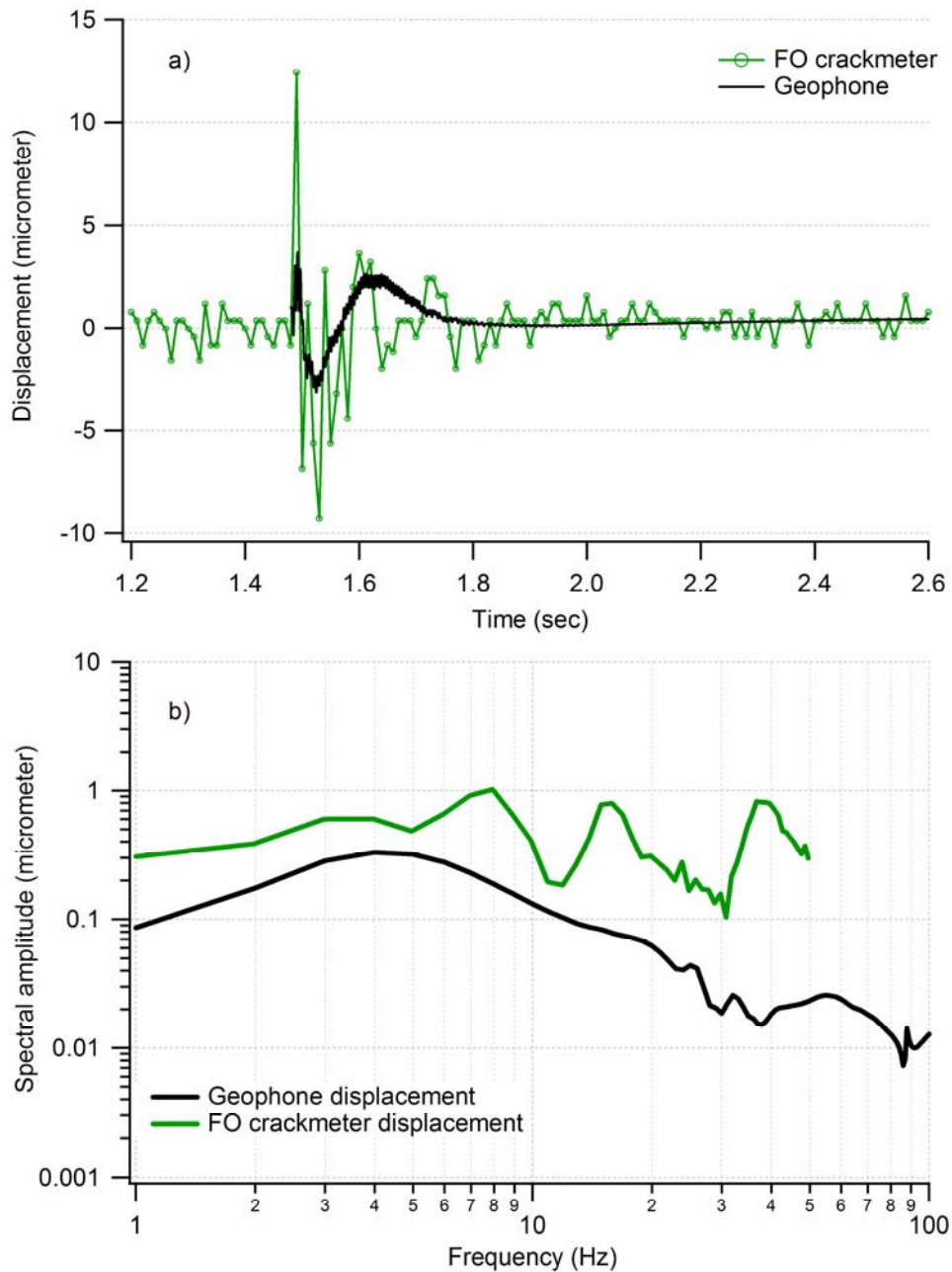
Figure 8: Dynamic test results: a) Time history of a shot at 2 m distance comparing the fiber optic crackmeter and the geophone ground motion response; b) Spectra for the same time interval. Low-frequency signals are represented fairly well by the fiber optic sensor, but the fiber optic record suffers from aliasing of higher frequency energy (greater than 50 Hz), which generates an apparent ringing in the time history and false spectral peaks not related to ground motion.